ELSEVIER

Journal of Neuroscience Methods 118 (2002) 153–161

JOURNAL OF NEUROSCIENCE METHODS

www.elsevier.com/locate/jneumeth

Identification of determinism in noisy neuronal systems

Marc W. Slutzky [a,*], Predrag Cvitanovic [b], David J. Mogul [a,c]

[a] Department of Biomedical Engineering, Northwestern University, 2145 Sheridan Road, Evanston, IL 60208, USA
[b] Department of Physics and Astronomy, Northwestern University, Evanston, IL 60208, USA
[c] Department of Neurobiology and Physiology, Northwestern University, Evanston, IL 60208, USA

Received 24 August 2001; received in revised form 7 February 2002; accepted 7 February 2002

Abstract

Most neuronal ensembles are nonlinear excitable systems. Thus it is becoming common to apply principles derived from nonlinear dynamics to characterize neuronal systems. One important characterization is whether such systems contain deterministic behavior or are purely stochastic. Unfortunately, many methods used to make this distinction do not perform well when both determinism and high-amplitude noise are present which is often the case in physiological systems. Therefore, we propose two novel techniques for identifying determinism in experimental systems. The first, called short-time expansion analysis, examines the expansion rate of small groups of points in state space. The second, called state point forcing, derives from the technique of chaos control. The system state is forced onto a fixed point, and the subsequent behavior is analyzed. This technique can be used to verify the presence of fixed points (or unstable periodic orbits) and to assess stationarity. If these are present, it implies that the system contains determinism. We demonstrate the use and possible limitations of these two techniques in two systems: the Hénon map, a classic example of a chaotic system, and spontaneous epileptiform bursting in the rat hippocampal slice. Identifying the presence of determinism in a physiological system assists in the understanding of the system's dynamics and provides a mechanism for manipulating this behavior.

Keywords: Chaos; Determinism; Nonlinear dynamics; Epilepsy; Bursting; Hippocampus; Noise

1. Introduction

The emerging field of nonlinear dynamics has opened up new avenues for the analysis of biological systems. One intriguing question to neuroscientists is whether a neuronal system's behavior is guided by some internal rules (i.e. is deterministic and hence predictable) or is purely random in nature. Because biological data are inherently noisy, however, many standard measures of nonlinear dynamics, e.g. correlation dimension and Lyapunov exponents, have not proven very reliable in characterizing biological systems (Theiler et al., 1992; Theiler, 1995). Other techniques have been used to either argue for the presence of determinism in experimental data (Kaplan, 1994; Aitken et al., 1995; Pueyo, 1997; Grassberger et al., 1991), or against it (Chang et al., 1994; Schiff et al., 1994a; Petracchi, 1997). However, most of these methods rely on either very long time series or low noise.

Lyapunov exponents measure sensitivity to initial conditions, a necessary condition for chaos, and hence are frequently used to quantify chaos in a system. Many methods have been developed to calculate Lyapunov exponents, including some developed especially for noisy data (Rosenstein et al., 1993; Kantz, 1994). Kantz' method in particular looks at the expansion rates of small neighborhoods of points localized in state space and averages them out over time. However, in our previous experiments, this method was not found to provide meaningful information for short-time series with a great deal of noise or extremely rapid expansion (Slutzky et al., 2001). In the case of short data sets recorded from in vitro bursting experiments in rat hippocampi, it was necessary to use larger initial neighborhoods to obtain enough initial points for the method to work correctly. These larger neighborhoods then expanded to the size of the entire attractor so

* Corresponding author. Tel.: +1-847-869-6207; fax: +1-847-967-7984
E-mail address: mslutzky@md.northwestern.edu (M.W. Slutzky).

0165-0270/02/$ - see front matter
PII: S0165-0270(02)00029-8

quickly that it was impossible to calculate an accurate average expansion rate.

Therefore, we have developed an alternative measure of expansion rates that approximates a maximal Lyapunov exponent. This method, which we shall refer to as short-time expansion (STE), measures the rate of spread among nearby points in state space after only one time step. It averages this rate of spread over the entire 'attractor' (i.e. all the points in the data set) which reduces the effects of local noise on the computations. Thus, it is a global measure of the mean expansion rate over the entire state space. We then compare this global expansion rate of the data with that of randomized surrogates of the data. Since a deterministic system should expand at a slower rate than a stochastic system (if the amplitude of the noise is comparable to the size of the attractor), this comparison enables us to identify the presence of determinism in the data. This might seem counterintuitive—a strong deterministic expansion rate might be expected to overpower noise—however, this is clearly not the case for short lengths of time where deterministic expansion rate is small but noise would be of the same amplitude no matter how short the time.

STE allows detection of determinism on a global scale. Another indicator of determinism, this one on a local scale, is the presence of unstable periodic orbits (UPOs) in a system (Auerbach et al., 1987). A periodic orbit is a set of points in state space to which a system returns repeatedly. A fixed point is a period-1 orbit (i.e. the system remains at that point over time). Saddle fixed points (the type most likely to be found in excitable systems) have an associated set of stable and unstable manifolds which can be approximated as straight lines in state space within a small distance of the fixed point. Points along the stable manifold are attracted to the fixed point, while points along the unstable manifold are repelled by the fixed point. A chaotic trajectory in state space can be thought of as wandering along a skeleton of UPOs (Auerbach et al., 1987). A few methods of detecting UPOs have been developed (Pierson and Moss, 1995; So et al., 1997), but they are time-intensive and may not be ideal for real-time applications such as chaos control. Another previously published method (Christini and Kaplan, 2000) uses chaos control to detect fixed points, but requires a great deal of stimulation and system perturbation, which may not be ideal for neural systems. We have developed a technique, referred to hereafter as state point forcing (SPF), that can validate fixed point (i.e. period-1 orbit) detection. It does this by forcing the system state point onto the fixed point estimate and then analyzing the system's behavior. This technique can help assess the stationarity of the system over the course of an experiment and indicate whether chaos control of a system is feasible—if the system remains close to the fixed point for a while, then it should be possible to manipulate the system into desired regions of behavior.

2. Methods

2.1. Experimental methods

Male Sprague–Dawley rats, age 20–25 days, were anesthetized (Isoflurane) and decapitated. Hippocampi were dissected out while perfused with chilled artificial cerebrospinal fluid (ACSF) containing (in mM): NaH_2PO_4 1.25, $MgSO_4$ 1.3, NaCl 124, $NaHCO_3$ 24, D-Glucose 10, KCl 3.5, $CaCl_2$ 2.4. Transverse slices 400 μm thick were cut using a tissue chopper (Stoelting) and maintained in oxygenated ACSF at room temperature. Slices were placed in the bottom of a 1 ml experimental bath under a dissecting microscope and perfused by oxygenated ACSF. The bath temperature was kept at 35 ± 1 °C, at a flow rate of 5–6 ml/min. A glass micropipette recording electrode (3–5 MΩ) was filled with 2 M NaCl and placed in the pyramidal layer of the CA3 region (Fig. 1A). Bursting was induced by bathing the slices in ACSF containing either high potassium (10.5 mM) or zero magnesium (Fig. 1B). Signals from the recording electrode were bandpass filtered on an AC differential amplifier (DAM 80, World Precision Instruments) with cutoff frequencies of 0.3 Hz and 3 kHz. For expansion rate analysis, bursts were recorded in AxoBASIC (Axon Instruments) and detected offline using a threshold-detection algorithm. Further details of experimental procedure were described in Slutzky et al. (2001).

For SPF experiments, a bipolar tungsten stimulating electrode was placed in the Schaffer collaterals. Stimuli consisted of single, 80 μs square-wave current pulses with amplitudes of 0.1–0.3 mA. Bursts were detected using an analog threshold-detection circuit. The threshold was set in the range 60–400 mV, depending on the noise amplitude in each experiment, and it was kept constant throughout each experiment. The interburst intervals (IBIs) were delay-embedded in two-dimensional (2D) state space (Sauer, 1995); i.e. the current and previous IBIs were plotted against each other as in a return map (Fig. 1C).

2.2. Analysis methods

The following sections describe our methods to extract information about underlying deterministic dynamics in situations where the noise is comparable in magnitude to the suspected deterministic dynamics. Our mathematical investigations stop whenever the quality of the data warrants no further refinement of the method; consequently questions about relations of these

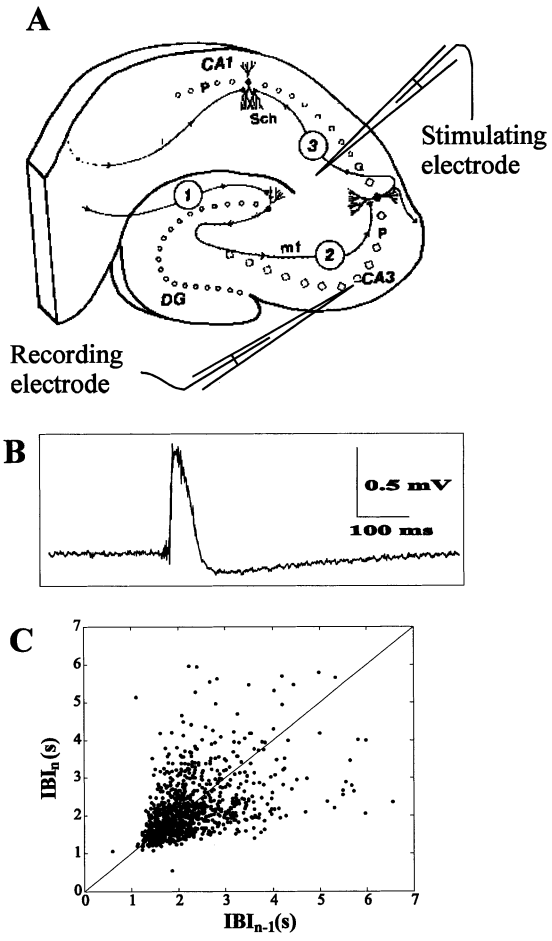

Fig. 1. Hippocampal slice burst activity. (A) Recording electrodes were placed in the CA3 stratum pyramidale (P) and stimulating electrode in the Schaffer collaterals. (B) An example of a spontaneous burst induced using high-$[K^+]_o$ solution. (C) A return map of 1000 IBIs from a spontaneous bursting experiment.

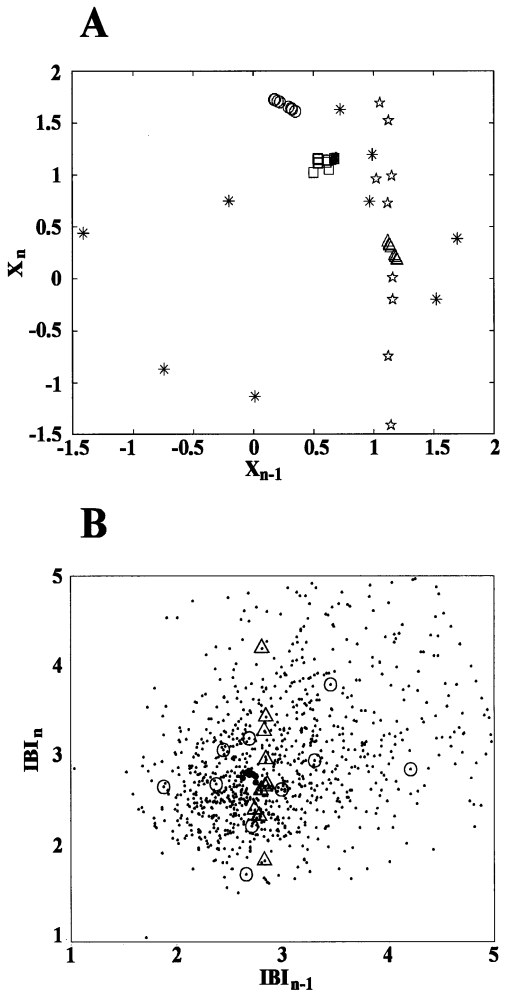

Fig. 2. An example of the rapid expansion of local neighborhoods in return maps of the data. (A) In the Hénon map, the initial points (solid dots) stay relatively close together after one (triangles) and two iterates (large circles). Randomized surrogates of Hénon expand very rapidly ($\square \rightarrow \star \rightarrow *$), as expected. (B) In contrast, in high-$[K^+]_o$ bursting data the initial neighborhood (large dots) expands in one step (triangles) to cover over half of the attractor, and in two steps (large circles) covers most of the entire attractor (seen as small dots).

methods to others which work well primarily for noise-less systems are not pursued here in depth.

2.2.1. Short-time expansion rate analysis

As described earlier, STE endeavors to surmount the obstacle of extremely rapid expansion (Fig. 2) by examining the ratio of distances between nearby points after only one time step. A given number of nearest neighbors was found for every point in the data set. The resulting cloud of points was then fit to an ellipse using principal components analysis (PCA). The largest principal component measures the variance along the major axis of the best-fit ellipse, and we used the square root of this component (i.e., the standard deviation) as a measure of the initial spread between the points. The points in the neighborhood were then evolved one iterate into the future. These points were again fit to an ellipse using PCA, and the variance along the major axis was obtained. The square root of the ratio of the two largest principal components then provided a measure of the one-step expansion rate. The local Lyapunov exponent could be estimated by the natural logarithm of this rate. The global expansion rate (L_{ave}) was then obtained by averaging the local estimates. That is,

$$L_{ave} = \sum_{i=1}^{N} \frac{\lambda_i}{N}, \qquad \lambda_i = \ln\left(\sqrt{\frac{p_1}{p_0}}\right), \tag{1}$$

where p_0 and p_1 are the largest principle components of the initial and iterated clouds of points, respectively; N is the total number of points in the data set; and λ_i is the local expansion rate. It was expected that after only one time step small neighborhoods of points would not spread out as quickly in deterministic systems as they would in strongly stochastic systems. If the system

contained a large stochastic component, the points would likely spread out over most if not all of the attractor after only one time step. Also, additive (extrinsic) noise should average out in this calculation leaving primarily the deterministic component. Therefore, L_{ave} should be smaller for a deterministic system than for a stochastic system.

L_{ave} varied with the number of neighbors included in each local estimate. This relationship was examined by computing L_{ave} for each data set using numbers of neighbors (NN) ranging from four to the total number of points in the data set. For both stochastic and deterministic systems, L_{ave} should decline logarithmically to zero as NN rises to the total number of points in the data set, since the neighborhood will have less and less room to expand. Also, in experimental systems, at very small NN noise levels are usually greater than the neighborhood size, so L_{ave} should decline logarithmically to zero for small NN as well. However, for a deterministic system, there should be some intermediate region where L_{ave} is relatively constant, which would imply a constant expansion rate is present. This idea enables us to discriminate determinism from noise by comparing the L_{ave} vs. NN relationship for a data set with that of corresponding surrogate data.

The STE rate analysis is not a method for evaluating Lyapunov exponents. It does that only for 1D maps; the expansion rate determined by our method is a derivation of a Lyapunov exponent as defined by the ergodic hypothesis, which replaces a long-time average with a one-step expansion rate weighted by natural measure. However, in higher dimensions the STE rate analysis does not yield the Lyapunov exponents, as an average of the magnitude of the leading expanding eigen value of one one-step stability matrix has no precise relation to the asymptotic time Lyapunov exponent. All one assumes is that if the flow is unstable almost everywhere, the STE rate is also positive, and roughly of the order of the leading Lyapunov exponent. Even if the true dynamics is high-dimensional, the Lyapunov exponent computed from its projection on a small-dimensional subspace is expected to be the same as the leading Lyapunov exponent. Representations of the dynamics in higher-dimensional subspaces would then enable us to estimate the smaller Lyapunov exponents.

The nature of our neuronal data does not appear to warrant investigations of embeddings of dynamics in dimensions higher than two primarily because we are barely able to extract a leading expansion rate exponent in the noisy Hénon map, and we see none in the experimental data. Intuitively, noise is infinite-dimensional, and for a deterministic flow with weak additive noise, an embedding dimension exceeding some level yields the situation where only the noise determines the size of the signal. For levels of noise measured in our neuronal data, the first time-delay map shows expansion that is barely consistent with determinism, and there is little opportunity for extracting any more information from higher-dimensional embeddings.

2.2.2. The method of surrogate data

The method of surrogate data was first developed (Theiler et al., 1992) as a way of testing for nonlinearities in time series. It has since been adapted as a method of determining the significance of other measures of nonlinearity calculated from time series, such as Lyapunov exponents (Theiler, 1995) or nonlinear prediction (Aitken et al., 1995). We used surrogate data to test for determinism in the STE rate analysis. Each surrogate data set was generated from the data by randomly shuffling the order of the IBIs according to a Gaussian distribution (Theiler et al., 1992). The surrogate data represented the null hypothesis that the experimental data could be explained by a linear stochastic process. If the L_{ave} vs. NN curve for the original data was significantly different from the average curve computed for the surrogates, then the null hypothesis could be rejected and the likelihood of determinism being present would be strengthened.

2.2.3. State point forcing

SPF is based on the chaos control paradigm. The goal of chaos control is to convert the system from a chaotic behavior to a periodic one by capitalizing on the presence and properties of UPOs in chaotic systems. In particular, period-1 orbits, or fixed points, are sought out using a UPO transform (UPOT) technique (So et al., 1997). This technique concentrates points tightly around the UPO so that the UPO shows up as a peak in a histogram of the transformed data. The statistical significance of this peak is then computed by comparing the data histogram with a distribution of histograms of surrogate data (to which the UPOT has also been applied). For real-time SPF protocols, only 10 data surrogates were used to calculate significance as compared to the 50 surrogates used for offline analysis (Slutzky et al., 2001). In the chaos control algorithm, when the system state point wanders far enough away from the fixed point, a stimulus is applied to shift the state point onto the stable manifold. The state point then will move in toward the fixed point along the stable manifold without further stimulation. This property minimizes the number of stimuli needed to maneuver the system into a periodic behavior.

In SPF, in contrast to chaos control, stimulation continued until the state point landed on the fixed point. Fixed points were first detected using the UPOT technique. Limitations in stimulus-burst interval precision occasionally interfered with exact placement of the state point onto the fixed point, so we required it to be within a very small distance of the fixed point. Since the goal of SPF was characterization, and not control, of

the system, minimizing the number of stimuli was not as high of a priority as in the chaos control algorithm. If the fixed point estimate were accurate, then the state point should remain near the fixed point on the subsequent iterate. However, if no fixed point existed or the fixed point estimate was inaccurate, then the subsequent state point could end up anywhere. We therefore, hypothesized that if we first forced the state point onto the fixed point and then forced it onto some other arbitrary point in the system attractor, the subsequent state points should in general stay closer to the fixed point than the arbitrary point. If the two cases were significantly different, it would imply that there was indeed a fixed point present near the estimate.

To measure the difference between these two cases, the system state point was forced onto the fixed (or arbitrary) point estimate 30–40 times (or one 'cycle'). This created a cluster of 'forced' points around the fixed point. We then computed the 2D mean of the cluster of points that were within the fixed point radius and the 2D mean of the subsequent iterates of these points. The difference of these two means was the change in the center of mass (ΔX_{cm}). If the system state were forced onto a true fixed point, then ΔX_{cm} would be small, while if it were forced onto some other arbitrary point or an inaccurate fixed point estimate, then ΔX_{cm} would be bigger. This idea is illustrated by Fig. 3. The case of forcing to a fixed point is shown in Fig. 3A, and the cluster of subsequent state points is shown in Fig. 3B. Since the subsequent iterates stay relatively close to the fixed point, ΔX_{cm} is small. When the system is forced to an arbitrary point, as in Fig. 3C and D, ΔX_{cm} is larger. Statistical comparisons of ΔX_{cm} were made with the paired t-test, or the Wilcoxon signed rank test when the data did not pass a normality test (SigmaStat, Jandel Scientific).

As stated above, the state point was forced onto the fixed point for a cycle and then onto an arbitrary point. The forcing point alternated between the fixed point and the arbitrary point from two to five cycles, until the fixed point seemed to be drifting due to nonstationarity. At this point, SPF was turned off and the fixed point was relocated using an adaptive tracking (AT) technique (Slutzky and Mogul, 2000). This technique was based on an algorithm designed to account for nonstationarity by readjusting the fixed point after each unstimulated burst (Christini and Kaplan, 2000). It used singular value decomposition to fit data to linear approximations of the dynamics in the neighborhood of the fixed point. This provided a new estimate of the fixed point and stable manifold. If a suitable fixed point estimate was found, then tracking was stopped and SPF resumed.

Both SPF and STE were first tested on the Hénon map, a classical chaotic system described by the equation:

$$x_{n+1} = 1 - 1.4x_n^2 + 0.3x_{n-1}. \quad (2)$$

Data from the Hénon map were delay-coordinate embedded in 2D in the same way as the IBI data.

3. Results

3.1. Short-time expansion analysis

STE was first tested on 1000 iterates of the Hénon map with and without added Gaussian noise and on 5 surrogates of each set of data. The values of L_{ave} for the surrogates were averaged. As shown in Fig. 4A, L_{ave} for the curve of the surrogate average decreased logarithmically to zero, while the curve of the noiseless Hénon system was nearly horizontal. The curve for the Hénon map with low noise ($\sigma = 0.02$) contained a large plateau in the range NN = 3–10% (of the points in the attractor), and the curve for larger noise ($\sigma = 0.2$, 7% of the attractor size) had a smaller plateau at NN = 10–20%. L_{ave} was slightly larger (0.50) than the accepted value of the Lyapunov exponent for the Hénon map (0.41, dashed line), but was reasonably close. As the noise amplitude increased, the curve started to resemble the curve of the surrogates.

STE analysis was then applied to 12 sets of IBI data recorded during spontaneous bursting experiments using high-$[K^+]_o$ or zero-$[Mg^{2+}]_o$ and to 5 surrogates of each data set. Plateau regions were not found in any of the bursting data sets tested. Curves of the data were very similar to those of the corresponding surrogate average. Even in the experiment with the largest difference between data and surrogates, the data curve was almost parallel to the surrogate mean curve (Fig. 4B). However, the curve was displaced from the surrogates, which suggests that the data were less disordered than the surrogates.

3.2. State point forcing

The SPF protocol was first tested on the Hénon map to make sure it could distinguish valid fixed points. As Fig. 5A and B demonstrate, the subsequent state points clearly stayed closer to the forcing point when the system was forced to a fixed point than when it was forced to an arbitrary point, even with added noise (which inhibited fixed point detection accuracy). This difference (ΔX_{cm}) increased with the distance between the arbitrary and fixed points. SPF was then applied to a total of 102 fixed points in 22 bursting experiments (on 16 hippocampal slices). Once a fixed point was found, the state point was alternately forced onto either the fixed or arbitrary point for 30–40 IBIs each until the fixed point appeared to be drifting (Fig. 5C). Then SPF

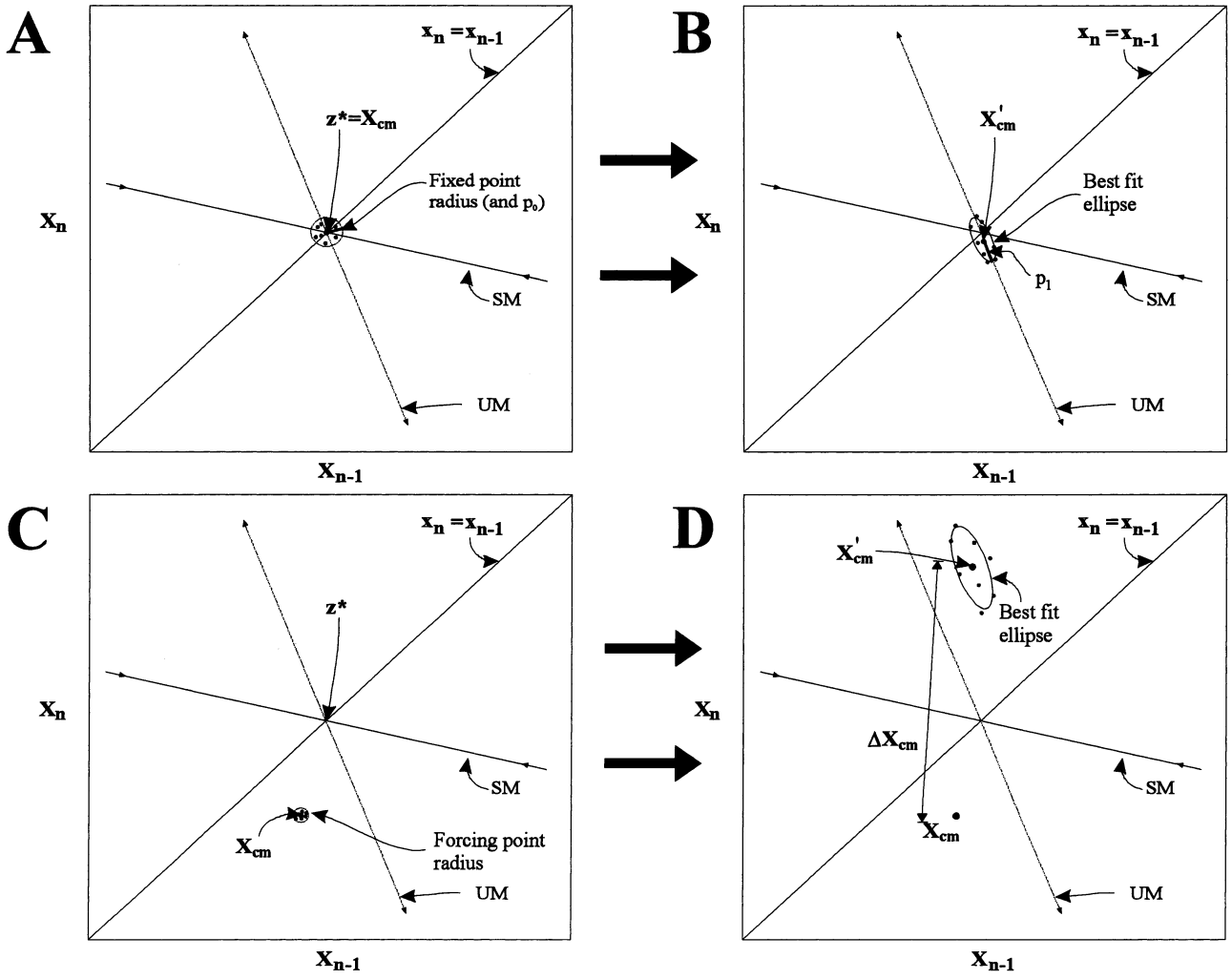

Fig. 3. A schematic of STE and SPF. (A) The system is forced to the fixed point z^*, producing a tight cluster of points around it (all within the fixed point radius). Thus, the center of mass X_{cm} equals the fixed point z^*. (B) The subsequent iterates of these points stay relatively close to the fixed point, and the new center of mass X'_{cm} stays relatively close to X_{cm}, so ΔX_{cm} is small. (C) When the system is forced to an arbitrary point far away from the fixed point, the cluster of points expands and moves (D), producing a large change in the center of mass ΔX_{cm}. In expansion rate analysis, the clusters of nearest neighbors around the fiducial point would be fit to ellipses using PCA (best-fit ellipse). The length of the major axis of this ellipse (p_1 in B) would then be compared to the major axis of the cluster of points (p_0 in A) to calculate the expansion rate. SM and UM are the stable and unstable manifolds, respectively.

was turned off and the AT technique was used to readjust the fixed point estimate (Section 2).

The value of ΔX_{cm} was computed for each fixed point and its corresponding arbitrary forcing point. There were 51 fixed point trials each of those detected with the UPOT and those found with the AT algorithm. The data were first compared for both UPO types combined, and ΔX_{cm} was significantly smaller when forcing to the fixed points than to the arbitrary points (median values 0.258 vs. 0.404 s, $P < 0.004$, signed rank test). When compared separately, the UPOT fixed points did not show a significant difference in ΔX_{cm} ($P = 0.07$), but the AT fixed points did have significantly smaller ΔX_{cm} when forcing to the fixed vs. arbitrary points (median values 0.22 vs. 0.38 s, respectively; $P < 0.015$).

The data were divided in several ways for further analysis. The arbitrary forcing point was set both higher than (positive) and lower than (negative) the fixed point in several trials. When it was set higher than the fixed point, the natural IBIs were sometimes shorter than the forcing point, so not enough data points could be obtained for the analysis. The arbitrary point was 0.1–0.4 s away (both positive and negative) from the fixed point, proportional to the size of the system attractor. The shift was typically 5–15% of the attractor width. The differences in ΔX_{cm} were significant when shifting negatively (0.18 vs. 0.41 s, fixed vs. arbitrary, respectively; $P < 0.0001$), but not when shifting positively ($P = 0.8$). The AT and UPOT fixed point data were then analyzed in the positive and negative shift categories.

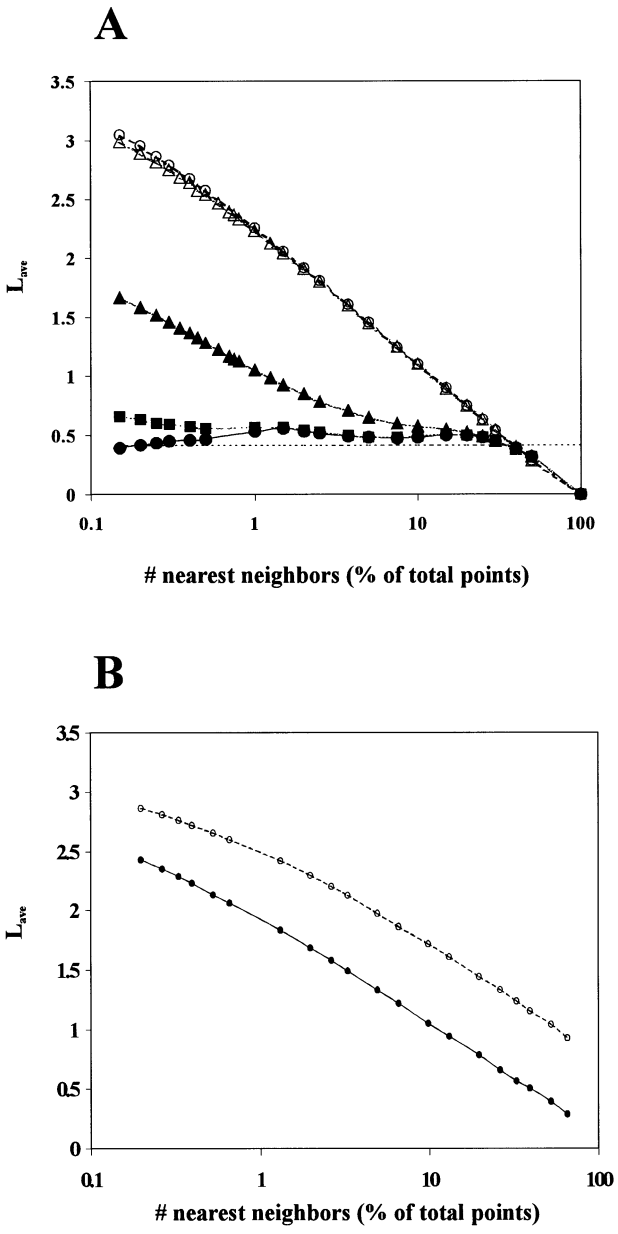

Fig. 4. Results of STE analysis in Hénon and bursting data from a high-$[K^+]_o$ experiment. (A) Curves of L_{ave} for the 2000-point Hénon map (●), the Hénon map with added Gaussian noise (■, $\sigma = 0.02$; ▲, $\sigma = 0.2$), and Gaussian-shuffled (SS) surrogates for noiseless (○) and noisy (△, $\sigma = 0.2$) Hénon map. L_{ave} for the surrogates decreases logarithmically with NN, but the noiseless and low-noise Hénon data curves are almost flat, and are close to the Lyapunov exponent for the Hénon map (0.415, dotted line). This shows an invariant expansion rate. With larger amounts of noise ($\sigma = 0.2$), the curve resembles the surrogates at small and large NN, but has a plateau in the NN = 5–20% range. (B) Curves of L_{ave} for one set of high-$[K^+]_o$ experimental data and corresponding SS surrogates. Curves for both data (●) and surrogates (○) decline logarithmically to zero with increasing NN. No plateaus are evident which indicates that the data are stochastic, with no evidence for determinism.

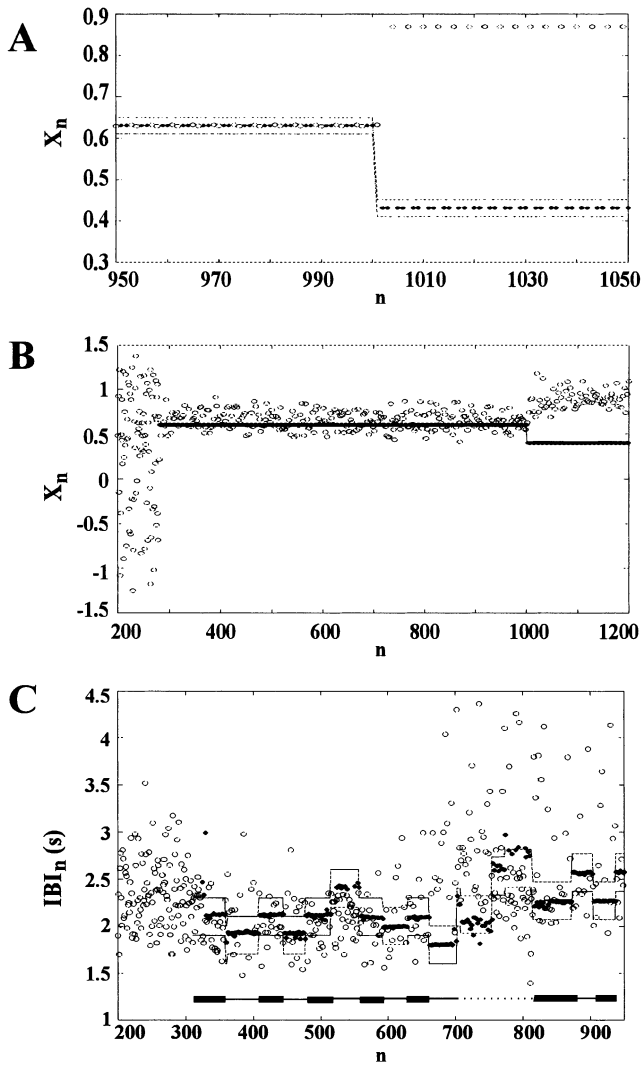

Fig. 5. Results from SPF analysis on Hénon and bursting data. When the system state wandered outside of the control region around the fixed point (dashed lines), the next burst would be triggered by an electrical stimulus. (A) In the noiseless Hénon system, the fixed point was found at 0.63. The system state was forced to it until $n = 1000$; then the system state was forced to a point 0.2 away from the fixed point. As expected, when the system was forced to the fixed point estimate by stimulating (●), the subsequent (unstimulated, ○) iterates stayed very close to the fixed point. But when the system state was forced to an arbitrary point (at 0.43), the subsequent iterates were up near 0.9. This same result was seen when increasing amounts of noise were added, even up to $\sigma = 0.1$ (B). (C) In this bursting experiment, forcing alternated between the fixed (thick lines) and arbitrary (thin lines) points 4 times. Then tracking was turned on (dotted line, starting at $n \approx 700$) until a new fixed point was found at $n = 820$. Tracking was then stopped and forcing resumed. The subsequent state points stayed closer to fixed points than to arbitrary points.

Again, negative shifts were significantly different for both AT ($P < 0.0001$) and UPOT ($P < 0.04$), while positive shifts were not significantly different for either. The data were broken down further by grouping according to the size of shift (from fixed to arbitrary point); the shift sizes ranged from −0.4 to +0.4. However, the number of trials in each group were almost all too small to produce enough power to detect

a significant difference. The exception to this was for shifts of −0.2, for which there were 24 trials. In this case, ΔX_{cm} was significantly smaller for the fixed than for the arbitrary point ($P < 0.002$).

4. Discussion

Two novel techniques for detecting determinism in noisy experimental systems have been introduced here. STE calculates average expansion rates over short periods of time and serves as a global measure of determinism. SPF uses a variant of chaos control to validate fixed point estimates obtained from other detection algorithms. These methods were used to analyze the mathematical Hénon map and the experimental bursting models of epilepsy. STE analysis identified deterministic behavior in the Hénon system with added noise but not in the bursting system which contained a great deal of noise. SPF analysis identified fixed points and hence determinism in both Hénon and bursting models.

Most of the existing methods for detecting deterministic behavior are not reliable for situations in which the system is very noisy and the amount of data is small. STE and SPF both were able to distinguish determinism present in the Hénon system under these restrictions. The choice of surrogate in this manuscript biased STE toward ruling out linear stochastic processes. No surrogate can completely model all types of stochastic noise. We were able to reject the null hypothesis for the Hénon system, however, a different type of stochastic process may still have been present.

The fact that STE did not detect determinism in bursting is probably due to the very high amount of noise present in addition to determinism. Because STE is a global measure, it may miss some local deterministic behavior if noise levels are very large (Slutzky et al., 2001). However, in a rapidly expanding system like hippocampal bursting, it is one of the few tools available to globally characterize the system. It appears that hippocampal bursting may either be too noisy or expand too rapidly for even STE to distinguish determinism. The results of SPF support prior analyses based on UPO detection (So et al., 1998; Slutzky et al., 2001) that suggested that there is indeed some determinism present in bursting at least on a local scale.

Fixed points are difficult to detect in noisy and short data sets, and the possibility of false-positive fixed point detections has been raised (T. Schreiber, personal communication). SPF provides an additional way to build confidence in fixed point estimates. The accuracy of these estimates is critical for the successful implementation of chaos control, since the premise of control is to keep the system close to a fixed point. For biological systems, this is particularly important, since they exhibit a high degree of nonstationarity, which causes fixed points to drift or disappear very rapidly. Other algorithms, e.g. the So UPOT, are time-intensive and require compromises to be made in accuracy in order to optimize speed for real-time applications. SPF allows estimates to be made relatively quickly in real-time. For those interested in controlling chaotic systems, SPF may provide a benchmark of whether this control is possible by revealing whether the fixed point estimates are sufficiently accurate and whether the system will stay close to the fixed point long enough to attain control.

The question of whether a neural system contains determinism or is completely random has important implications. Some evidence against determinism has been found in spinal cord reflex circuits (Chang et al., 1994) and hippocampal circuits (Schiff et al., 1994a). Other studies have been published that suggest that neuronal activity (Braun et al., 1999), specifically hippocampal bursting (So et al., 1998; Slutzky et al., 2001), does contain determinism. If the system contains determinism, that implies that it behaves according to certain rules and is theoretically predictable for a short-time, even if it is chaotic. This property could be very useful; for example, it could allow the ability to predict or even prevent an epileptic seizure (Schiff et al., 1994b; Aitken et al., 1995; Lehnertz and Elger, 1998; Slutzky et al., in press). The two new tools described here should provide additional flexibility to experimental researchers seeking to answer this question about their system.

References

Aitken PG, Sauer T, Schiff SJ. Looking for chaos in brain slices. J Neurosci Meth 1995;59:41–8.

Auerbach D, Cvitanovic P, Eckmann J-P, Gunaratne G, Procaccia I. Exploring chaotic motion through periodic orbits. Phys Rev Lett 1987;58:2387–9.

Braun HA, Dewald M, Schafer K, Voigt K, Pei X, Dolan K, et al. Low-dimensional dynamics in sensory biology 2: facial cold receptors of the rat. J Comp Neurosci 1999;7:17–32.

Chang T, Schiff SJ, Sauer T, Gossard JP, Burke RE. Stochastic versus deterministic variability in simple neuronal circuits: I. Monosynaptic spinal cord reflexes. Biophys J 1994;67:671–83.

Christini DJ, Kaplan DT. Adaptive estimation and control method for unstable periodic dynamics in spike trains. Phys Rev E 2000;61:5149–53.

Grassberger P, Schreiber T, Schaffrath C. Nonlinear time sequence analysis. Int J Bif Chaos 1991;1:521–47.

Kantz H. A robust method to estimate the maximal Lyapunov exponent. Phys Lett A 1994;185:77–87.

Kaplan DT. Exceptional events as evidence for determinism. Physica D 1994;73:38–48.

Lehnertz K, Elger CE. Can epileptic seizures be predicted? Evidence from nonlinear time series analysis of brain electrical activity. Phys Rev Lett 1998;80:5019–22.

Petracchi D. The search for periodic unstable orbits in periodically driven spike trains. Chaos Solit Fract 1997;8:327–34.

Pierson D, Moss F. Detecting periodic unstable points in noisy chaotic and limit cycle attractors with applications to biology. Phys Rev Lett 1995;75:2124–7.

Pueyo S. The study of chaotic dynamics by means of very short time series. Physica D 1997;106:57–65.

Rosenstein MT, Collins JJ, De Luca CJ. A practical method for calculating largest Lyapunov exponents from small data sets. Physica D 1993;65:117–34.

Sauer T. Interspike interval embedding of chaotic signals. Chaos 1995;5:127–32.

Schiff SJ, Jerger K, Chang T, Sauer T, Aitken PG. Stochastic versus deterministic variability in simple neuronal circuits: II. Hippocampal slice. Biophys J 1994a;67:684–91.

Schiff SJ, Jerger K, Duong DH, Chang T, Spano ML, Ditto WL. Controlling chaos in the brain. Nature 1994b;370:615–20.

Slutzky MW, Cvitanovic P, Mogul DJ. Deterministic chaos and noise in three in vitro hippocampal models of epilepsy. Ann BME 2001;29:607–18.

Slutzky MW, Cvitanovic P, Mogul DJ. Manipulating epileptiform bursting in the rat hippocampus using chaos control and adaptive techniques. IEEE Trans BME, in press.

Slutzky MW, Mogul DJ. Modification of epileptiform bursting using chaos control. Proceedings of World Congress on Medical Physics and BME, 2000.

So P, Francis J, Netoff TI, Gluckman B, Schiff SJ. Periodic orbits: a new language for neuronal dynamics. Biophys J 1998;74:2776–85.

So P, Ott E, Sauer T, Gluckman BJ, Grebogi C, Schiff SJ. Extracting unstable periodic orbits from chaotic time series data. Phys Rev E 1997;55:5398–417.

Theiler J. On the evidence for low-dimensional chaos in an epileptic electroencephalogram. Phys Lett A 1995;196:335–41.

Theiler J, Eubank S, Longtin A, Galdrikian B, Farmer JD. Testing for nonlinearity in time series: the method of surrogate data. Physica D 1992;58:77–94.